J Solid State Electrochem (2012) 16:3307–3313
DOI 10.1007/s10008-012-1776-6

ORIGINAL PAPER

Synthesis of $Li_4Ti_5O_{12}$ fibers as a high-rate electrode material for lithium-ion batteries

Li Wang · Qizhen Xiao · Zhaohui Li · Gangtie Lei · Ping Zhang · Lijuan Wu

Received: 22 November 2011 / Revised: 12 May 2012 / Accepted: 14 May 2012 / Published online: 26 May 2012

Abstract Porous lithium titanate ($Li_4Ti_5O_{12}$) fibers, composed of interconnected nanoparticles, are synthesized by thermally treating electrospun precursor fibers and utilized as an energy storage material for rechargeable lithium-ion batteries. The material is characterized by X-ray diffraction, scanning electron microscopy, high-resolution transmission electron microscopy, and thermal analysis. Scanning electron microscopy results show that the $Li_4Ti_5O_{12}$ fibers calcined at 700 °C have an average diameter of 230 nm. Especially, the individual fiber is composed of nanoparticles with an average diameter of 47.5 nm. Electrochemical properties of the material are evaluated using cyclic voltammetry, galvanostatic cycling, and electrochemical impedance spectroscopy. The results show that as-prepared $Li_4Ti_5O_{12}$ exhibits good cycling capacity and rate capability. At the charge–discharge rate of 0.2, 0.5, 1, 2, 10, 20, 40, and 60 C, its discharge capacities are 172.4, 168.2, 163.3, 155.9, 138.7, 123.4, 108.8, and 90.4 mAh g^{-1}, respectively. After 300 cycles at 20 C, it remained at 120.1 mAh g^{-1}. The obtained results thus strongly support that the electrospun $Li_4Ti_5O_{12}$ fibers could be one of the most promising candidate anode materials for lithium-ion batteries in electric vehicles.

Keywords Electrospinning · Porous fibers · Anode · Lithium-ion batteries

Q. Xiao · P. Zhang (✉)
College of Civil Engineering & Mechanics, Xiangtan University,
Xiangtan, Hunan 411105, China
e-mail: zhangp@xtu.edu.cn

L. Wang · Q. Xiao · Z. Li · G. Lei · L. Wu
Key Laboratory of Environmentally Friendly Chemistry
and Applications of Ministry of Education, College of Chemistry,
Xiangtan University,
Xiangtan, Hunan 411105, China

Q. Xiao (✉)
College of Chemistry, Xiangtan University,
Xiangtan, Hunan 411105, China
e-mail: qizhenxiao2004@yahoo.com.cn

Introduction

Lithium-ion batteries have attracted attention as power supplies of electric vehicles and hybrid electric vehicles due to its high power, high energy density, and long cycle life [1–3]. The spinel lithium titanate ($Li_4Ti_5O_{12}$) has been demonstrated as a potential candidate for the anode electrode material in high-power Li-ion batteries as well as hybrid electric vehicles [4–13]. It has good structural stability with an almost negligible volume change during the discharge–charge processes, which suggests good Li-ion insertion and extraction reversibility and long cycle life. However, one practical problem associated with $Li_4Ti_5O_{12}$ anode is its poor rate performance at high charge–discharge rates mainly due to its low electronic conductivity (only 10^{-13} S cm^{-1} at 20 °C). To overcome this problem, it is important to design and fabricate nanostructured electrode materials that provide high interface area between the metal oxide and electrolyte and short diffusion paths for ionic transport and electronic conduction during charging and discharging [14, 15].

Generally speaking, various synthesis methods such as sol–gel route [16], hydrothermal synthesis [17], molten salt process [18], and so on have been proposed to prepare nanostructured $Li_4Ti_5O_{12}$ electrode materials. For example, Li et al. [8] have reported one-dimensional $Li_4Ti_5O_{12}$ prepared by hydrothermal method that exhibits high rate performance. Kang et al. [9] have reported a mesostructured spinel

$Li_4Ti_5O_{12}$/carbon nanocomposite via block copolymer self-assembly that shows a reversible capacity of 115 mAh g^{-1} with 90 % capacity retention after 500 cycles at 10 C. Kim et al. [10] reported that a spinel $Li_4Ti_5O_{12}$/reduced graphite composite prepared by a two-step microwave-assisted solvothermal reaction and heat treatment yields excellent rate capability and cycling performance. In order to improve the electrochemical performances during cycling, nanocrystalline $Li_4Ti_5O_{12}$ was synthesized by a single-step solution combustion method, previously described by Prakash et al. [19]. As we are known, nanoelectrode materials composed of one-dimensional nanowires for lithium-ion batteries by electrospinning [20, 21] have shown great advantages over other processing methods. The electrospinning approach provides a flexible way to prepare large-scale nanomaterials to fulfill the requirements for electrode materials. Chan et al. reported that the electrodes composed of one-dimensional nanowires could bring significant improvement in the electrochemical performance, attributing the increased performance to a better strain relaxation and firm electronic contact during charge–discharge cycles [22, 23]. Lu et al. [24] reported that spinel $Li_4Ti_5O_{12}$ nanofibers with 3D net architecture were prepared by electrospinning, exhibiting good cycle stability. Guo et al. [25] have reported that $Li_4Ti_5O_{12}$/C fibers were synthesized through the electrospinning method, which exhibited high reversible capacity and great rate capability.

In this work, we successfully synthesized porous $Li_4Ti_5O_{12}$ fibers through an electrospinning method and high-temperature thermal treatment. The morphology, crystal structure, and electrochemical properties of $Li_4Ti_5O_{12}$ fibers were systematically investigated. The individual fiber is composed of nanoparticles; it produces porous interconnected nanoparticle network which would provide higher electrode/electrolyte contact surface and better electronic and ionic conductivity. The results of electrochemical measurements indicate that the anode material made of $Li_4Ti_5O_{12}$ fibers exhibits excellent cycling stability and high rate capability.

Experimental section

Materials preparation

The $Li_4Ti_5O_{12}$ fibers were prepared by combining the sol–gel chemistry and electrospinning technique. The solution for electrospinning was prepared from tetrabutyl titanate (TBT), lithium acetate (LiOAc), polyvinyl pyrrolidone (PVP, M_W=1,300,000), ethanol, and acetic acid. All chemicals were obtained from Aldrich. TBT (3.00 g), CH_3COO-$Li{\cdot}2H_2O$ (0.72 g), PVP (0.79 g), and acetic acid (3.0 mL) were added to the ethanol solvent (15.5 mL). The mixture was stirred for 24 h to obtain the precursor solution. Subsequently, the precursor solution was loaded into a one-off injector with a spinneret made of stainless steel. The distance between the spinneret and the collector was 20 cm, and the applied voltage was 28 kV. The precursor solution was fed by a pump at a rate of 0.25 mL h^{-1}. The electrospun fibers were dried in air at 100 °C overnight, and then calcined at different temperature (600, 700, 750, and 800 °C) for 12 h at a heating rate of 1 °C min^{-1} in air to obtain $Li_4Ti_5O_{12}$.

Characterizations

The surface morphologies were investigated by scanning electron microscopy (SEM; JEOL JSM-6360) and high-resolution transmission electron microscopy (TEM; JEOL 3010). The crystal structures of $Li_4Ti_5O_{12}$ calcined at different temperatures were determined by X-ray diffraction (XRD; Rigaku D/max 2550) pattern (Cu Kα radiation) in the range of 10–80° at a scan rate of 10° min^{-1}. The thermal behavior of the gel precursor was characterized by thermogravimetry (TG) and differential thermal analysis in the SDTQ 600 instrument ranged from room temperature to 800 °C at a heating rate of 10 °C min^{-1} in air.

Electrochemical measurement

The electrode was prepared by using 70 wt% of $Li_4Ti_5O_{12}$ as active materials, 20 wt% carbon black and 10 wt% polyvinylidene difluoride as binder, which were dissolved in *N*-methyl-2-pyrrolidinone. The obtained slurry was then coated onto the copper foil current collectors and dried for 12 h in a vacuum oven at 120 °C. The coin cell (CR2016) was fabricated using the lithium metal as a counter electrode and reference electrode. The electrolyte was 1 mol L^{-1} solution of $LiPF_6$ in a mixture of 1:1 (*v*/*v*) ethylene carbonate and diethyl carbonate. The separator (Celgard 2400) was soaked in an electrolyte for 24 h prior to use. Coin cell assembly was carried out in an argon-filled glove box by keeping both the moisture content and oxygen level less than 1 ppm. The charge–discharge measurements were carried out in the voltage range of 2.0–1.0 V at different rates, which were performed through a NEWARE BTS-5 V10 mA computer-controlled battery test station at different rates of 0.2–60 C. The capacity was based on the amount of the active material, excluding the weight of the additives in the electrode. The cyclic voltammetry (CV) was performed on a Potentiostat/Galvanostat M273 in conjunction with M5210 Lock-in amplifier instrument (Princeton Applied Research & AMTECT Company). The electrochemical impedance spectroscopy was also investigated by the Potentiostat/Galvanostat M273 in conjunction with the M5210 Lock-in amplifier instrument with an AC voltage of 5 mV amplitude in the frequency range from 1×10^{5} to 1×10^{-5} Hz.

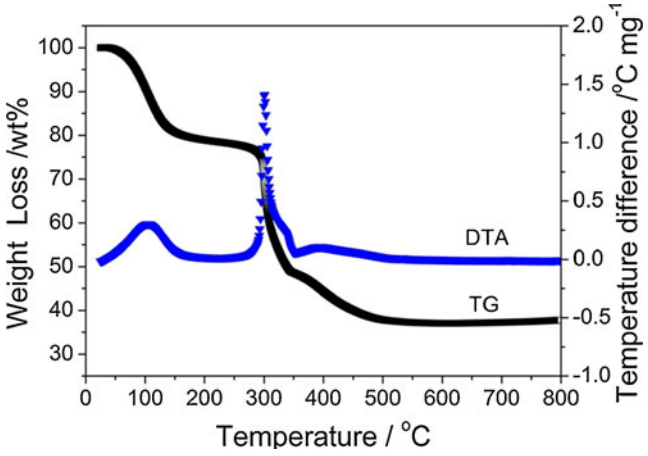

Fig. 1 TG/DTA curves of the electrospun LiOAc/TBT/PVP fibers at a heating rate of 10 °C min^{-1} in air

Results and discussion

Figure 1 shows the TG/DTA curves of the electrospun LiOAc/TBT/PVP precursor fibers at a heating rate of 10 °C min^{-1} under air atmosphere. It is found that there are two main endothermic peaks during heating the fibers from room temperature to 800 °C. The first endothermic peak can be ascribed to the evaporation heat of absorbed water from the precursor fibers at around 100 °C. The second endothermic peak (280–350 °C) may be relative to the thermal decomposition of lithium acetate, tetrabutyl titanate, and PVP. Subsequently, the curve is flat, and no endothermic peak is observed. For the TG curve, no obvious weight loss is also observed after 500 °C. The sample remains about 36.7 % of the initial weight when the temperature is higher than 500 °C. As shown in Fig. 1, the TG curve demonstrates that the annealing temperature must be higher than 550 °C to make the thermal reaction complete.

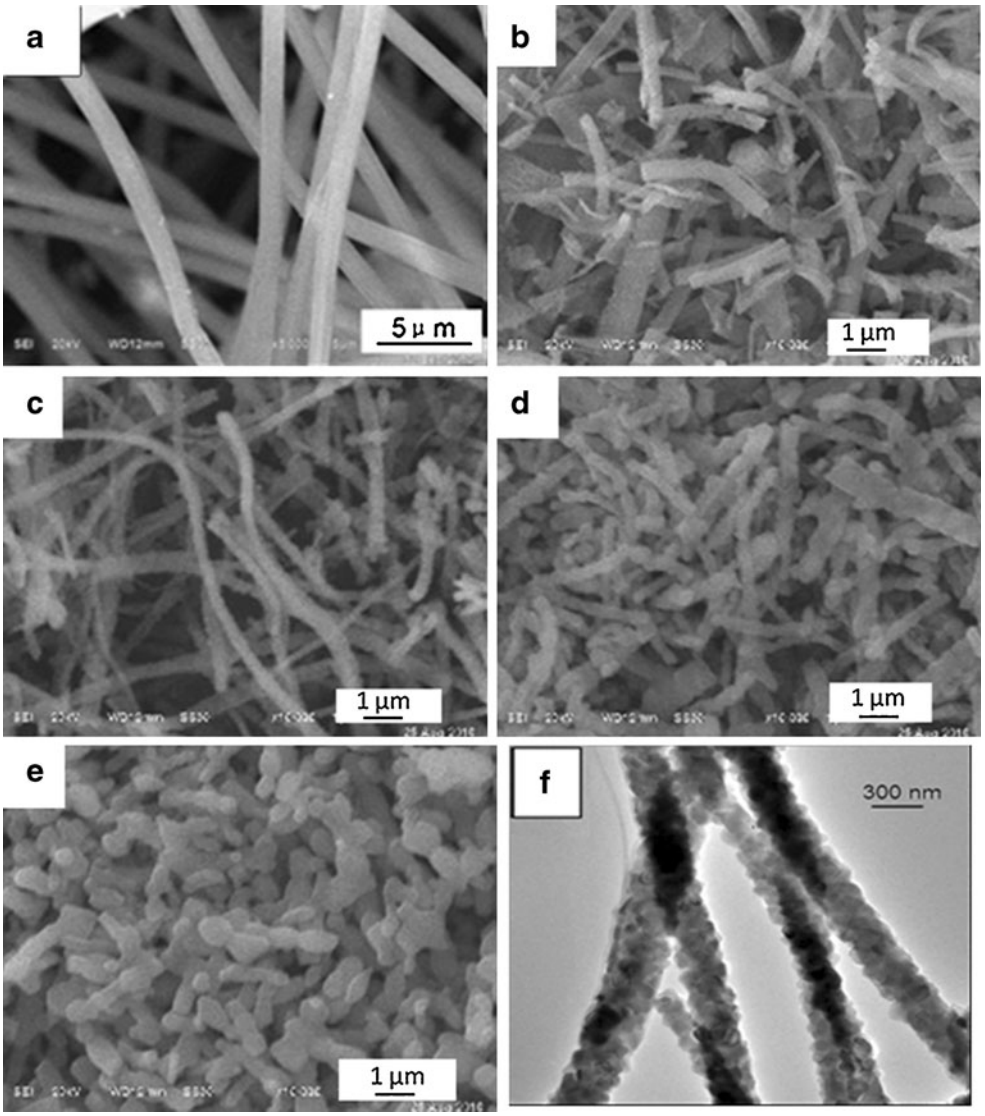

Fig. 2 **a** SEM image of electrospun LiOAc/TBT/PVP fibers, **b**–**e** SEM images of $Li_4Ti_5O_{12}$ which is synthesized at different temperatures (**b** 600, **c** 700, **d** 750, and **e** 800 °C), **f** TEM images of $Li_4Ti_5O_{12}$ fibers calcined at 700 °C

Figure 2a shows a SEM image of the electrospun LiOAc/TBT/PVP fibers. All fibers exhibit a long and straight morphology with relatively uniform diameters ranging from 400 to 600 nm, and no beads or fiber defect with so-called beads on a string morphology is observed. Figure 2b–e shows SEM images of $Li_4Ti_5O_{12}$ calcined at different temperatures [(b) 600, (c) 700, (d) 750, and (e) 800 °C]. The sample heated up to 700 °C could maintain the conventional electrospun fiber morphology. The diameter of fibers decreases after annealing at 700 °C due to the decomposition of lithium acetate, tetrabutyl titanate, and PVP in the electrospun fibers. It can be seen that there were a number of large size particles or particle aggregates after the fibers were calcined at 750 °C. As shown in Fig. 2e, it is obvious that there is a significant change in microstructure when increasing the calcination temperature to 800 °C, indicating that obvious melting occurs. Figure 2f shows the TEM image of $Li_4Ti_5O_{12}$ fibers calcined at 700 °C. The individual fiber with porous structure is composed of uniform interconnected nanoparticles with average diameter less of than 50 nm, which is consistent with the result of XRD. The possible mechanism behind the formation of these fibers is suggested in the schematic shown in Scheme 1. The thermal decomposition of lithium acetate, tetrabutyl titanate, and PVP occurs simultaneously under sintering; the sintering process has an effect on the growth of $Li_4Ti_5O_{12}$ nanoparticles and allows the nanoparticles to join together, forming porous fibers.

The cycling performances of $Li_4Ti_5O_{12}$ calcined at different temperatures are shown in Fig. 3. The $Li_4Ti_5O_{12}$ fibers calcined at 700 °C show the best cycling stability; a discharge capacity of 173.0 mAh g^{-1} is maintained at 0.2 C after 10 cycles. However, the $Li_4Ti_5O_{12}$ calcined at 600, 750, and 800 °C has discharge capacities of only 110, 110, and 132 mAh g^{-1} after 10 cycles, respectively. The experimental results indicate that $Li_4Ti_5O_{12}$ calcined at 700 °C has the best electrochemical performance. Thus, we choose 700 °C as the annealing temperature to obtain the $Li_4Ti_5O_{12}$ fibers, which could maintain the fibrous morphology and have excellent electrochemical performance.

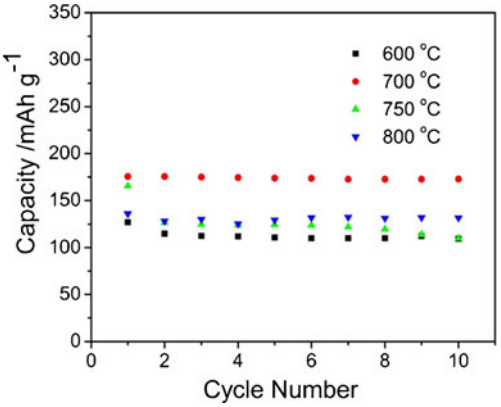

Fig. 3 The cycling performances of $Li_4Ti_5O_{12}$ calcined at different temperatures

The influence of calcination temperature on the formation of $Li_4Ti_5O_{12}$ was investigated. Figure 4 shows XRD patterns of the as-prepared $Li_4Ti_5O_{12}$ obtained by calcining the precursor fibers at different temperatures. It can be seen that the anatase TiO_2 and Li_2TiO_3 impurities are present when annealed at 600 °C. The existence of the impurities is related to the incomplete reaction of the precursor. When increasing the calcination temperature to 700 °C, the main diffraction peaks appear at 2θ=18.33°, 35.57°, and 43.24°, which can be attributed to (111), (311), and (400) reflections of the cubic structure of spinel $Li_4Ti_5O_{12}$ (JCPDS no: 49–0207) with Fd3m space group. A diffraction peak located at 2θ=27.38° is assigned to rutile TiO_2 impurity, although a trace amount of TiO_2 is still observed at very weak peak intensity. Such a trace of impurity phase is later found out to have a negligible effect on the electrode performance. This result suggests that the $Li_4Ti_5O_{12}$ can be facilely formed by calcining the precursor at 700 °C for 12 h. A detailed crystal line size (D) is calculated using a Scherrer equation $\beta\cos(\theta) = k\lambda/D$, where β is the half-peak width of the XRD diffraction peak, θ is the position of

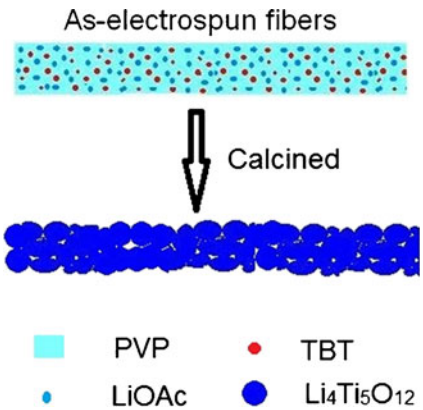

Scheme 1 A schematic diagram for the formation of porous $Li_4Ti_5O_{12}$ fibers during sintering

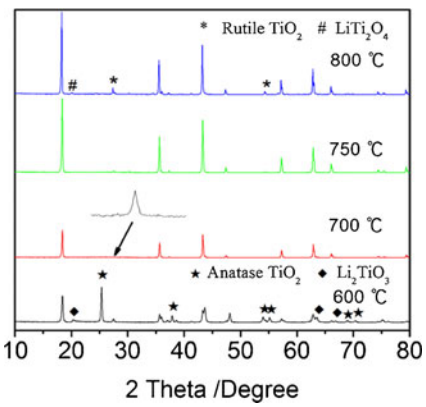

Fig. 4 XRD patterns of the as-prepared $Li_4Ti_5O_{12}$ at different temperatures (600, 700, 750, and 800 °C)

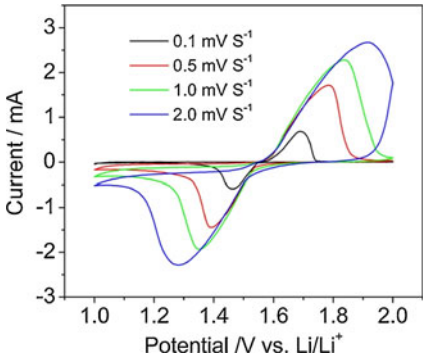

Fig. 5 The CV curves of the $Li_4Ti_5O_{12}$ electrode calcined at 700 °C in the voltage range of 2.0–1.0 V at different scan rates

the peak (2θ=18.33°), λ is wavelength of CuKα radiation, and k is a constant (0.89) [26]. It is found that the average crystalline size (D) of the nanoparticles is 47.5 nm, providing a short Li-ion diffusion path. Further increasing the calcination temperature to 750 °C, the intensities of the diffraction peaks increase, which indicate that the average crystallite size of the nanoparticles increases. When the temperature is 800 °C, the impurity phase rutile TiO_2 and $LiTi_2O_4$ appear which might be ascribed to the decomposition of $Li_4Ti_5O_{12}$. So, it can also be concluded that the 700 °C is an optimized calcination temperature to obtain $Li_4Ti_5O_{12}$ fibers.

Figure 5 shows the cyclic voltammograms of the $Li_4Ti_5O_{12}$ electrode calcined at 700 °C at different scan rates. A couple of redox peaks located at about 1.67 and 1.47 V (vs. Li/Li^+) are observed at a scan rate of 0.1 mV s^{-1}, which indicates the reversible Li^+ intercalation and de-intercalation in $Li_4Ti_5O_{12}$, namely, the redox reaction of Ti^{4+}/Ti^{3+}. The potential interval ΔE between the anodic and cathodic peaks increases when scan rate is increased gradually from 0.1 to 2 mV s^{-1}, which is caused by the polarization.

The profiles of voltage versus capacity at different rates for the $Li_4Ti_5O_{12}$ electrode calcined at 700 °C are shown in Fig. 6. The material shows an initial discharge capacity of

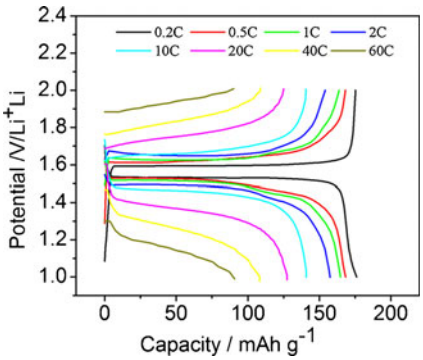

Fig. 6 The profiles of voltage versus capacity of the $Li_4Ti_5O_{12}$ electrode calcined at 700 °C at charge–discharge rates between 2.0 and 1.0 V

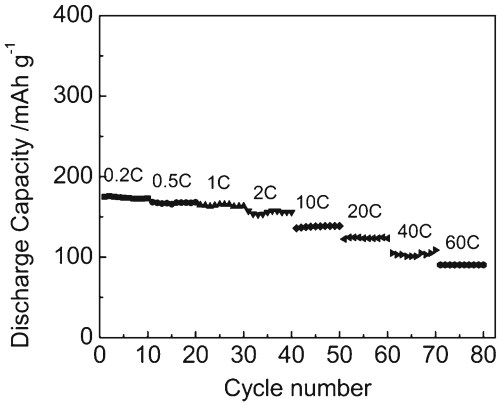

Fig. 7 Rate performances of the $Li_4Ti_5O_{12}$ calcined at 700 °C at different rates between 2.0 and 1.0 V

175.5 mAh g^{-1} and charge capacity of 174.5 mAh g^{-1} with 99 % the coulomb efficiency during the first charge and discharge cycle (0.2 C), and voltage plateaus (discharge and charge) appear at 1.53 and 1.60 V, respectively, which are consistent with the CV curves. By increasing gradually the galvanostatic charge–discharge rate from 0.2 to 60 C, the voltage plateaus of the discharge shift to lower potential, while the voltage plateaus of the charge shift to higher potential at higher rates due to kinetic effects of the material. In addition, when the charge–discharge rate is higher than 10 C, high polarization for the charge–discharge process occurs, which could be related to a more evident surface-confined charge transfer kinetics (known as the pseudocapacitive faradaic kinetics) and diffusion-controlled kinetics as lithium intercalating/deintercalating in $Li_4Ti_5O_{12}$ [27].

Figure 7 shows the cycling performance of $Li_4Ti_5O_{12}$ calcined at 700 °C at different discharge rates between 2.0 and 1.0 V. The galvanostatic charge–discharge rate was increased gradually from 0.2 to 60 C, 10 cycles for each rate. A specific discharge capacity of 173.0 mAh g^{-1} is obtained at a rate of 0.2 C after 10 cycles; the reversible discharge capacity of 168.2, 163.3, 155.9, 138.7, 123.4, 108.8, and 90.4 mAh g^{-1} is observed at a discharge rate of 0.5, 1, 2, 10, 20, 40, and 60 C in the last cycle, respectively.

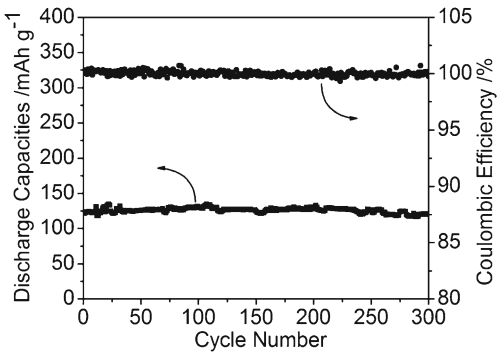

Fig. 8 Cycle performance of the $Li_4Ti_5O_{12}$ calcined at 700 °C at a rate of 20 C

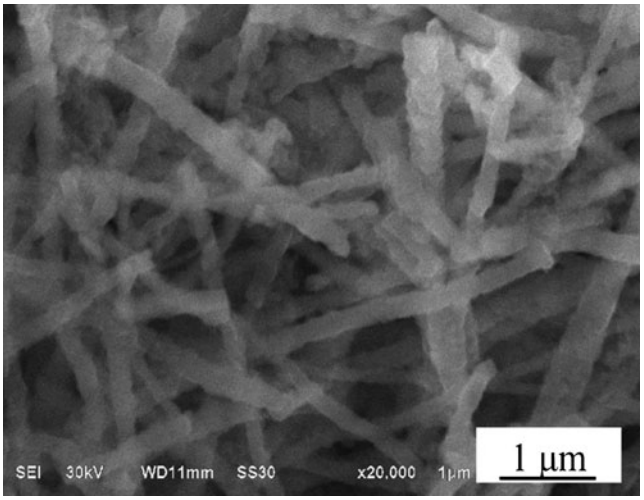

Fig. 9 SEM image of the $Li_4Ti_5O_{12}$ fibers electrode after 20 cycles

This rate capacity is higher than the recently reported for similar anode materials [28]. Such good rate capability results from its good electrode electronic contact and high surface area of the fibers, which is a high electrode–electrolyte contact area, resulting in improvement of both electron and Li^+ transport.

In order to further evaluate the electrochemical performance of the product, the variation of discharge capacity with cycle number at 20 C charge–discharge rate is shown in Fig. 8. It can be observed that the $Li_4Ti_5O_{12}$ shows a stable cycle life. The discharge capacity in the first cycle is 122.4 mAh g^{-1} at 20 C, and a capacity of 120.1 mAh g^{-1} is obtained after 300 cycles. The $Li_4Ti_5O_{12}$ electrode shows a capacity retention of 98.1 % of the first discharge capacity. Furthermore, as shown in Fig. 8, the coulombic efficiency remains almost at 100 %. These results show that lithium-ion intercalation into and deintercalation out of the $Li_4Ti_5O_{12}$ electrode are highly reversible. It can be seen that the $Li_4Ti_5O_{12}$ fibers have good cycling performance even at high current density.

Figure 9 shows the SEM image of the $Li_4Ti_5O_{12}$ fiber electrode calcined at 700 C. This sample went through 20 charge–discharge cycles at 1 °C with a cutoff range of 2.0–1.0 V. The SEM image shows essentially the same morphological features of the $Li_4Ti_5O_{12}$ fiber structures, which indicate that the fibrous morphology of $Li_4Ti_5O_{12}$ is not destroyed after lithium-ion intercalation/deintercalation into/out of the electrode. In all, the morphology change is essentially negligible after charge–discharge cycles, which corresponds to the excellent cycling performance.

Figure 10a shows the impedance spectra of $Li_4Ti_5O_{12}$ calcined at 700 °C, which were measured in the fully discharged state after cycling. The impedance spectra have two semicircles: one semicircle is in the high-to-medium frequency region and is attributed to the resistance of surface film (R_{sf}) covering on the particles, and the other is in the low-frequency region approximately and represents the charge transfer resistance (R_{ct}) [29]. The inclined lines in the lower frequency are attributed to the Warburg impedance, which is associated with lithium-ion diffusion in $Li_4Ti_5O_{12}$ electrode. The lithium-ion diffusion coefficient could be calculated using the following equation [29]: $D = R^2T^2/2A^2n^4F^4C^2\sigma^2$.

Herein, R is the gas constant, T is the absolute temperature, A is the surface area of the cathode, n is the number of electrons per molecule during oxidization, F is the Faraday constant, C is the concentration of lithium-ion (0.014 mol cm^{-3} for $x=1$), and σ is the Warburg factor which is associated with Z_{re}: $Z_{re} = R_e + R_{sf} + R_{ct} + \sigma\omega^{-1/2}$

Herein, R_e is the resistance of electrolyte, R_{sf} is the resistance of surface film, and R_{ct} is the charge transfer resistance. R_{ct} and R_{sf} are found to be 56 and 55 Ω, respectively, based on the fitted data using the equivalent circuit. Figure 10b shows the relationship plot between Z_{re} and reciprocal square root of the angular frequency ($\omega^{-1/2}$) at low-frequency region. The lithium-ion diffusion coefficient of $Li_4Ti_5O_{12}$ was calculated, and is 3.14×10^{-11} cm^2 s^{-1}, which is higher than that of the recently reported [30]. In addition, an electric conductivity of 2.1×10^{-7} S cm^{-1} is obtained for the $Li_4Ti_5O_{12}$ fibers (measured by a four-point probe method). These results exhibit that the porous fiber structure allows better lithium-ions diffusion and electronic conductivity, which is in good agreement with the rate capability.

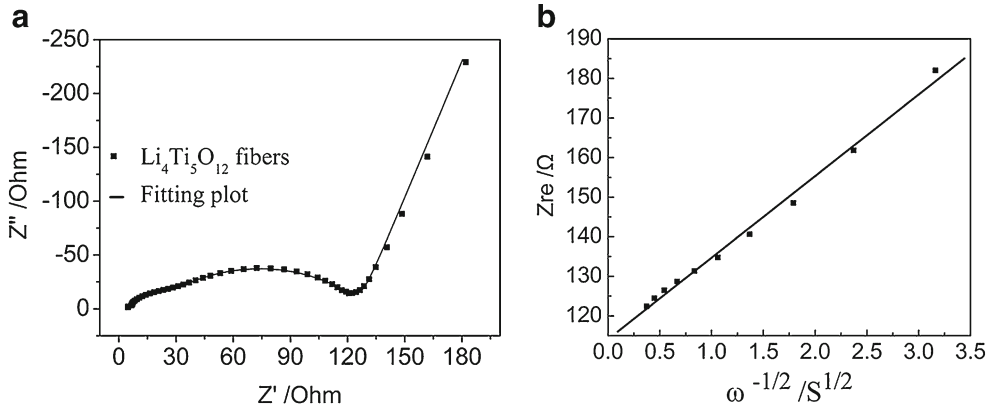

Fig. 10 **a** The impedance spectra of the $Li_4Ti_5O_{12}$ calcined at 700 °C, and **b** the relationship plot between Z_{re} and $\omega^{-1/2}$ at low-frequency region

Conclusions

Porous $Li_4Ti_5O_{12}$ fibers, composed of interconnected nanoparticles, have been successfully synthesized via electrospinning method followed by thermal treatment. The $Li_4Ti_5O_{12}$ fibers calcined at 700 °C have an average diameter of 230 nm. Especially, the individual fiber is composed of nanoparticles with an average diameter of 47.5 nm. Electrochemical measurements indicate that the anode material made of the $Li_4Ti_5O_{12}$ fibers displays a highly reversible capacity and excellent rate capability, which is due to the short lithium diffusion path and high electric conductivity of $Li_4Ti_5O_{12}$ fibers.

Acknowledgments This work was financially sponsored by the National Post-Doctoral Fund of China (no. 20090461013), the postdoctoral fund of Xiangtan University, and the Open Fund from Key Laboratory of Advanced Functional Polymeric Materials of Hunan Province (no. AFPM200906), the project of Science and Technology of Hunan Province (no. 2010RS4012).

References

1. Endo M, Kim C, Nishimura K, Fujino T, Miyashita K (2000) Carbon 38:183–197
2. Scrosati B (1995) Nature 373:557–558
3. Nelson RF (2000) J Power Sources 91:2–26
4. Guerfi A, Sévigny S, Lagacé M, Hovington P, Kinoshita K, Zaghib K (2003) J Power Sources 119–121:88–94
5. Scharner S, Weppner W, Schmid-Beurmann P (1999) J Electrochem Soc 146:857–861
6. Jiang C, Ichihara M, Honma I, Zhou H (2007) Electrochim Acta 52:6470–6475
7. Cheng L, Yan J, Zhu GN, Luo JY, Wang CX, Xia YY (2010) J Mater Chem 20:595–602
8. Li JR, Tang ZL, Zhang ZT (2005) Electrochem Commun 7:894–899
9. Kim HK, Bak SM, Kim KB (2010) Electrochem Commun 12:1768–1771
10. Prakash AS, Manikandan P, Ramesha K, Sathiya M, Tarascon JM, Shukla AK (2010) Chem Mater 22:2857–2863
11. Cui W, He YB, Tang ZY, Yang QH, Xu Q, Su FY, Ma L (2011) J Solid State Electrochem. doi:10.1007/s10008-011-1316-9
12. He ND, Wang BS, Huang JJ (2010) J Solid State Electrochem 14:1241–1246
13. Zhao YM, Liu GQ, Liu L, Jiang ZY (2009) J Solid State Electrochem 13:705–711
14. Amatucci GG, Badway F, Pasquier AD, Zheng T (2001) J Electrochem Soc 148:A930–A939
15. Cheng L, Liu HJ, Zhang JJ, Xiong HM, Xia YY (2006) J Electrochem Soc 153:A1472–A1477
16. Dokko K, Sugaya J, Nakano H, Yasukawa T, Matsue T, Kanamura K (2007) Electrochem Commun 9:857–862
17. Chen J, Yang L, Fang S, Tang Y (2010) Electrochim Acta 55:6596–6600
18. Rahman MM, Wang JZ, Hassan MF, Chou SL, Wexler D, Liu HK (2010) J Power Sources 195:4297–4303
19. Kang E, Jung YS, Kim GH, Chun J, Wiesner U, Dillon AC, Kim JK, Lee J (2011) Adv Funct Mater 21:4349–4357
20. Yu Y, Gu L, Wang CL, Dhanabalan A, Van Aken PA, Maier J (2009) Angew Chem Int Ed 48:6485–6489
21. Kim C, Yang KS, Kojima M, Yoshida K, Kim YJ, Kim YA, Endo M (2006) Adv Funct Mater 16:2393–2397
22. Chan CK, Zhang XF, Cui Y (2008) Nano Lett 8:307–309
23. Chan CK, Peng H, Liu G, Mcllwrath K, Zhang XF, Huggins RA, Cui Y (2008) Nat Nanotechnol 3:31–35
24. Lu HW, Zeng W, Li YS, Fu ZW (2007) J Power Sources 164:874–879
25. Guo B, Li Y, Yao Y, Lin Z, Ji L, Xu G, Liang Y, Shi Q, Zhang X (2011) Solid State Ionics 204–205:61–65
26. Venkateswara Rao C, Rambabu B (2010) Solid State Ionics 181:839–843
27. Xu R, Li J, Tang Z, Zhang Z (2011) J Nanomater. doi:10.1155/2011/635416
28. Li G, Xia J, Jiao J, Chen L, Shen P (2011) Chin J Chem 29:1824–1828
29. Liao XZ, Ma ZF, Gong Q, He YS, Pei L, Zeng LJ (2008) Electrochem Commun 10:691–694
30. Chen JZ, Yang L, Fang SH, Hirano S, Tachibana K (2011) J Power Sources. doi:10.1016/j.jpowsour.2011.10.052